doi:10.1088/0004-637X/787/1/55

OUTBURSTING COMET P/2010 V1 (IKEYA–MURAKAMI): A MINIATURE COMET HOLMES

MASATERU ISHIGURO[1,2], DAVID JEWITT[2,3], HIDEKAZU HANAYAMA[4], FUMIHIKO USUI[5], TOMOHIKO SEKIGUCHI[6],
KENSHI YANAGISAWA[7], DAISUKE KURODA[7], MICHITOSHI YOSHIDA[8], KOUJI OHTA[9], NOBUYUKI KAWAI[10],
TAKESHI MIYAJI[4], HIDEO FUKUSHIMA[4,11], AND JUN-ICHI WATANABE[4,11]

[1] Department of Physics and Astronomy, Seoul National University, Gwanak, Seoul 151-742, Korea
[2] Department of Earth, Planetary and Space Sciences, University of California at Los Angeles,
595 Charles Young Drive East, Los Angeles, CA 90095-1567, USA
[3] Department of Physics and Astronomy, University of California at Los Angeles, 430 Portola Plaza, Box 951547, Los Angeles, CA 90095-1547, USA
[4] Ishigakijima Astronomical Observatory, National Astronomical Observatory of Japan, Ishigaki, Okinawa 907-0024, Japan
[5] Department of Astronomy, Graduate School of Science, The University of Tokyo, 7-3-1 Hongo, Bunkyo-ku, Tokyo 113-0033, Japan
[6] Department of Teacher Training, Hokkaido University of Education, 9 Hokumon, Asahikawa 070-8621, Japan
[7] Okayama Astrophysical Observatory, National Astronomical Observatory of Japan, Asaguchi, Okayama 719-0232, Japan
[8] Hiroshima Astrophysical Science Center, Hiroshima University, 1-3-1 Kagamiyama, Higashi-Hiroshima, Hiroshima 739-8526, Japan
[9] Department of Astronomy, Kyoto University, Kyoto 606-8502, Japan
[10] Department of Physics, Tokyo Institute of Technology, 2-12-1 Ookayama, Meguro-ku, Tokyo 152-8551, Japan
[11] National Astronomical Observatory of Japan, Mitaka, Tokyo 181-8588, Japan
Received 2014 January 30; accepted 2014 April 3; published 2014 May 2

ABSTRACT

The short-period comet P/2010 V1 (Ikeya–Murakami, hereafter "V1") was discovered visually by two amateur astronomers. The appearance of the comet was peculiar, consisting of an envelope, a spherical coma near the nucleus and a tail extending in the anti-solar direction. We investigated the brightness and the morphological development of the comet by taking optical images with ground-based telescopes. Our observations show that V1 experienced a large-scale explosion between UT 2010 October 31 and November 3. The color of the comet was consistent with the Sun ($g' - R_C = 0.61 \pm 0.20$, $R_C - I_C = 0.20 \pm 0.20$, and $B - R_C = 0.93 \pm 0.25$), suggesting that dust particles were responsible for the brightening. We used a dynamical model to understand the peculiar morphology, and found that the envelope consisted of small grains (0.3–1 μm) expanding at a maximum speed of 500 ± 40 m s^{-1}, while the tail and coma were composed of a wider range of dust particle sizes (0.4–570 μm) and expansion speeds 7–390 m s^{-1}. The total mass of ejecta is $\sim 5 \times 10^8$ kg and kinetic energy $\sim 5 \times 10^{12}$ J. These values are much smaller than in the historic outburst of 17P/Holmes in 2007, but the energy per unit mass (1×10^4 J kg^{-1}) is comparable. The energy per unit mass is about 10% of the energy released during the crystallization of amorphous water ice suggesting that crystallization of buried amorphous ice can supply the mass and energy of the outburst ejecta.

Key words: comets: general – comets: individual (P/2010 V1) – interplanetary medium – meteorites, meteors, meteoroids

Online-only material: color figures

1. INTRODUCTION

The periodic comet P/2010 V1 (Ikeya–Murakami, hereafter V1) was independently discovered by two amateur astronomers in Japan, Mr. Kaoru Ikeya and Dr. Shigeki Murakami, in early 2010 November (Nakano & Ikeya 2010a). They reported the comet to be at a magnitude of 8–9 at the time of discovery. Later, the orbital elements (semimajor axis $a = 3.083$ AU, eccentricity $e = 0.488$, and inclination $i = 9°.38$) showed that V1 is a short-period comet with an orbital period of 5.41 yr (Williams 2010). Figure 1 shows the orbit projected on the ecliptic plane. It has a Tisserand parameter with respect to Jupiter, $T_J = 3.013$, slightly larger than 3. Such comets are sometimes classified as Encke-type comets (2P/Encke has $T_J = 3.026$) rather than Jupiter-family comets, for which $2 \leqslant T_J < 3$ (Levison & Duncan 1997). Despite its short orbital period and considerable brightness at the time of discovery, it is interesting to note that V1 had not previously been detected.

To date, there are no published reports to characterize the physical properties of V1. Images taken by amateur astronomers showed interesting features. The comet was enveloped by a spherical cloud and the overall appearance was reminiscent of historic cometary outbursts in 17P/Holmes. To characterize the physical properties, we obtained monitoring observations and compared them with a model based on the dynamics of dust grains.

2. OBSERVATIONS AND DATA REDUCTION

The data presented in this study were obtained with three telescopes: the Ishigakijima Astronomical Observatory Murikabushi 1.05 m telescope (hereafter IAO), the Keck I 10 m telescope (Keck-I), and the Indian Institute of Astrophysics (IIA) 2.0 m Himalayan Chandra telescope (HCT). A journal of the observations is given in Table 1. Details of the data acquisition and reduction are given in the following.

Long-term monitoring observations of V1 were taken at IAO, in Okinawa, Japan with the Murikabushi 1.05 m Ritchey–Chrétien telescope (F/12) with a focal reducer and MITSuME, a system to take contemporaneous images with three different filters of SDSS g', Johnson–Cousins R_C, and I_C-band. Each of the three cameras utilizes an Alta U6 (Apogee Instruments, Inc.) CCD with array size of 1024 × 1024 pixels and with pixel size of 24 × 24 μm. The effective wavelengths and the FWHM are $\lambda_e = 4830$ Å and $\Delta\lambda = 1340$ Å

Table 1
Observation Log

Date	UT	Observatory (Instrument)	Filter (Exptime[a])	Seeing[b]	r_h[c]	Δ[d]	α[e]
2010 Nov 9	20:32–21:02	IAO (MITSuME)	g' (26), R_C (27), I_C (27)	3.4	1.60	2.32	20.3
2010 Nov 20	20:25–21:12	IAO (MITSuME)	g' (26), R_C (38), I_C (38)	2.5	1.62	2.29	21.7
2010 Nov 26	20:24–21:14	IAO (MITSuME)	g' (28), R_C (45), I_C (45)	4.2	1.63	2.27	22.5
2010 Dec 2	20:13–21:23	IAO (MITSuME)	g' (66), R_C (66), I_C (66)	3.3	1.67	2.24	24.1
2010 Dec 12	20:25–21:12	IAO (MITSuME)	g' (42), R_C (42), I_C (42)	2.4	1.68	2.23	24.4
2010 Dec 19	20:37–21:28	IAO (MITSuME)	g' (48), R_C (48), I_C (48)	2.5	1.70	2.20	25.2
2011 Jan 30	15:48–15:55	KECK-I (LRIS)	B (4.6), R_C (3.7)	1.0	1.87	2.03	28.9
2011 Fab 4	19:41–21:25	IAO (MITSuME)	g' (80), R_C (80), I_C (80)	4.8	1.90	2.00	29.1
2011 Mar 29	21:44–23:28	HCT (HFOSC)	R_C (63)	3.0	2.17	1.68	26.3

Notes.
[a] Total effective exposure time in minutes.
[b] FWHM seeing in arcsec.
[c] Median heliocentric distance in AU.
[d] Median geocentric distance in AU.
[e] Median Solar phase angle (Sun–V1–observer angle) in degree.
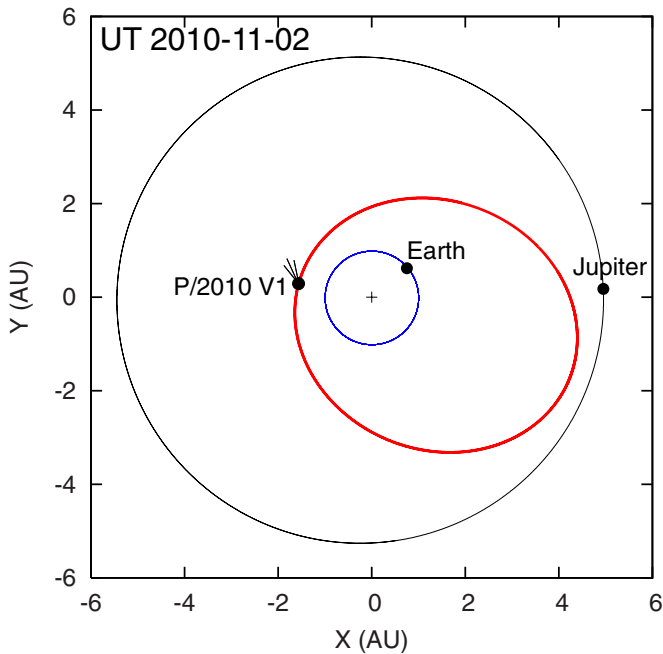
Figure 1. Orbits of P/2010 V1 (Ikeya–Murakami) projected on the ecliptic plane. Large ellipse is the orbit of Jupiter, and the small ellipse is the orbit of the Earth. Cross denotes the position of the Sun, and filled circles show the positions of the comet, Earth, and Jupiter on UT 2010 November 2, a potential date of the outburst. This is shown in the heliocentric ecliptic coordinate, that is, the x-axis points from the Sun toward the vernal equinox and y-axis completes the right-hand ecliptic coordinate system.

(A color version of this figure is available in the online journal.)

(g'), $\lambda_e = 6550$ Å and $\Delta\lambda = 1210$ Å (R_C), and $\lambda_e = 7990$ Å and $\Delta\lambda = 1570$ Å (I_C). In this configuration, the pixel size projected on the sky was 0″.72 and the field of view was 12′.3 × 12′.3. The observations were made using non-sidereal tracking in sky conditions that were variable through our observation runs.

Multiband snapshots were obtained with the 10 m Keck I telescope atop Mauna Kea on UT 2011 January 30. Images were taken using the Low Resolution Imaging Spectrometer (LRIS) camera (Oke et al. 1995), which houses red and blue optimized

CCDs separated by a dichroic filter (we used the 460 dichroic, which has 50% transmission at 4875 Å). The image scale on both cameras was 0″.135 per pixel and the available field-of-view was 5′.3 × 7′.3. The telescope was tracked at sidereal rates owing to temporary failure of the Keck guider control software. We secured two sets of images simultaneously in the B-band ($\lambda_e = 4370$ Å and $\Delta\lambda = 900$ Å) and R-band ($\lambda_e = 6800$ Å and $\Delta\lambda = 1270$ Å) filters, with exposures of 25 s and 20 s for the first set and 250 s and 200 s for the second set, respectively. We used the first set because the comet was trailed due to the sidereal tracking in the second set. The sky above Mauna Kea was photometric.

The last observation for V1 was carried out on UT 2011 March 29 with the 2.0 m Ritchey–Chrétien HCT located at 4500 meters in the Himalayan region, India. It is operated by the Indian Astronomical Observatory, the IIA. We employed the Himalaya Faint Object Spectrograph (HFOSC) 2048 × 4096 pixel CCD camera with R_C-band filter ($\lambda_e = 6550$ Å and $\Delta\lambda = 1450$ Å) at the f/9 Cassegrain focus of the telescope. The image scale on the camera was 0″.296 per pixel and the available field-of-view was $10' \times 10'$. The observation was conducted in a crowded region of stars at the galactic longitude and latitude of 354°.4 and −1°.5. We could not detect the comet with the HCT but used these data to place an upper limit to the brightness.

The raw images were reduced in the standard manner for CCD data. The bias data were obtained at intervals throughout each night. We used median-stacked data frames to construct flat-field images with which to correct for pixel-to-pixel variation in CCD response and vignetting. Flux calibration was obtained using standard stars in the Landolt catalog when available (Landolt 1992, 2009), otherwise we used field stars listed in the USNO–B1.0 catalog (Monet et al. 2003). We employed WCSTools to transform CCD pixel coordinates into celestial coordinates (Mink 1997). The estimated astrometric accuracy was about 0″.4, which is good enough to argue the position angle and morphology of dust structure in the following section. To remove cosmic rays and background objects such as galaxies and stars in IAO and HCT data, we followed a technique described in Ishiguro et al. (2007) and Ishiguro (2008). The technique is useful only when a number of exposures were acquired. For the Keck-I image, we did not delete stars because only one set of exposures was available.

Figure 2. $g'R_C I_C$-band composite color image of V1 taken on UT 2010 November 9. We allocated g'-band image as blue, R_C-band image as green, and I_C-band image as red to make the color image. The celestial north is up and celestial east to the left. The field-of-view of the image is $9' \times 9'$.

3. RESULTS

3.1. The Color

Figure 2 shows a false-color composite image taken on UT 2010 November 9. In the figure, we assigned a g'-band image as blue, a R_C-band image as green, and an I_C-band image as red. At a glance, the comet has a whitish color, suggesting that the intensity distribution is similar among these three bands. We derived the apparent magnitudes of the entire cloud on UT 2010 November 9 as $g' = 10.14 \pm 0.13$, $R_C = 9.53 \pm 0.14$, and $I_C = 9.33 \pm 0.14$. In addition, we measured the color of near-nucleus dust within an aperture of $1''$ in radius on 2011 January 30 using Keck-I images and derived $B - R_C = 0.93 \pm 0.25$. The color indices of the cloud, $g' - R_C = 0.61 \pm 0.20$ and $R_C - I_C = 0.20 \pm 0.20$ on November 9, and $B - R_C = 0.93 \pm 0.25$ on January 30, are consistent with those of the Sun, that is, $(g' - R_C)_\odot = 0.65$ (Kim et al. 2012), $(R_C - I_C)_\odot = 0.33$, and $(B - R_C)_\odot = 1.00$ (Holmberg et al. 2006). It is therefore natural to believe that scattered sunlight by dust particles accounted for a large fraction of the flux in the cloud.

Careful investigation enables us to find subtle differences between images taken in different filters. Based on inspection of the spectra of other comets, we assumed that the observed I_C-band intensity is wholly due to dust continuum, and then extracted a signal from other filters associated with emission lines from gaseous atoms and molecules excited to fluorescence by sunlight. Figure 3 shows the differential images on UT 2010 November 9. We forced a match to the brightness level of the observed envelope in each band in order to subtract the dust continuum. The comparison shows a spherical cloud in the g'-band image, centered on the nucleus. This cloud was not clear in R_C-band (less than a few percent of dust continuum). Spherical structures are often detected in comets, where they are attributed to C_2 (4500–4800 Å, 4900–5200 Å, and 5300–5600 Å) and NH_2 (4900–5000 Å, ~5200 Å, ~5400 Å, ~5700 Å, and
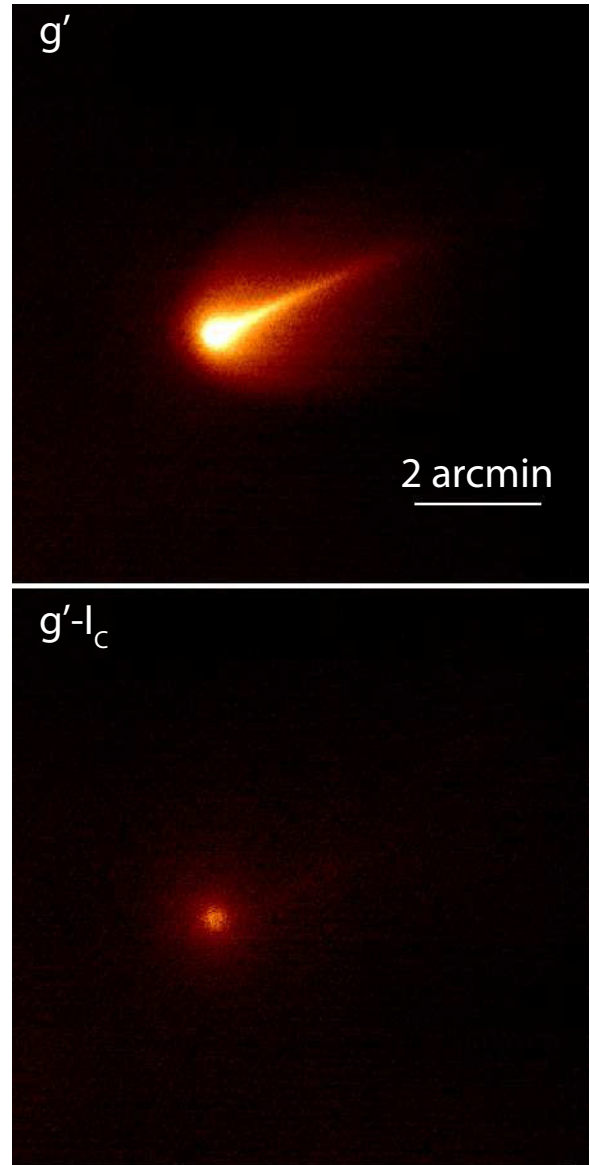

Figure 3. g'-band image (top) and differential intensity image between g' and R_C-bands image (i.e., g'-band intensity minus R_C-band intensity, bottom). The contribution of the spherical coma is about 10% of the signal near the nucleus. This image was taken on UT 2010 November 9. The orientation of these images are the same as Figure 2, that is, celestial north is up and celestial east to the left. The field-of-view of the image is $9' \times 9'$.

~6000 Å) (Capria et al. 2010; Brown et al. 1996; Combi & Delsemme 1980). For the subsequent analysis, we used the R_C-band images because they are more sensitive than I_C-band images while remaining less contaminated by gaseous emission than are g'-band images.

3.2. Time-evolution of Morphology

As mentioned above, the optical image showed a unique morphology of the dust cloud consisting of an envelope, a near-nucleus coma, and a tail (see Figure 2). Figure 4 shows the time-series R_C-band images of V1 from UT 2010 November 9 to UT 2011 March 29. Note that the smudge-like features in Figures 4(c)–(e) are artifacts of off-axis scattered light from Venus. The envelope was clear in the first image (Figure 4(a)),
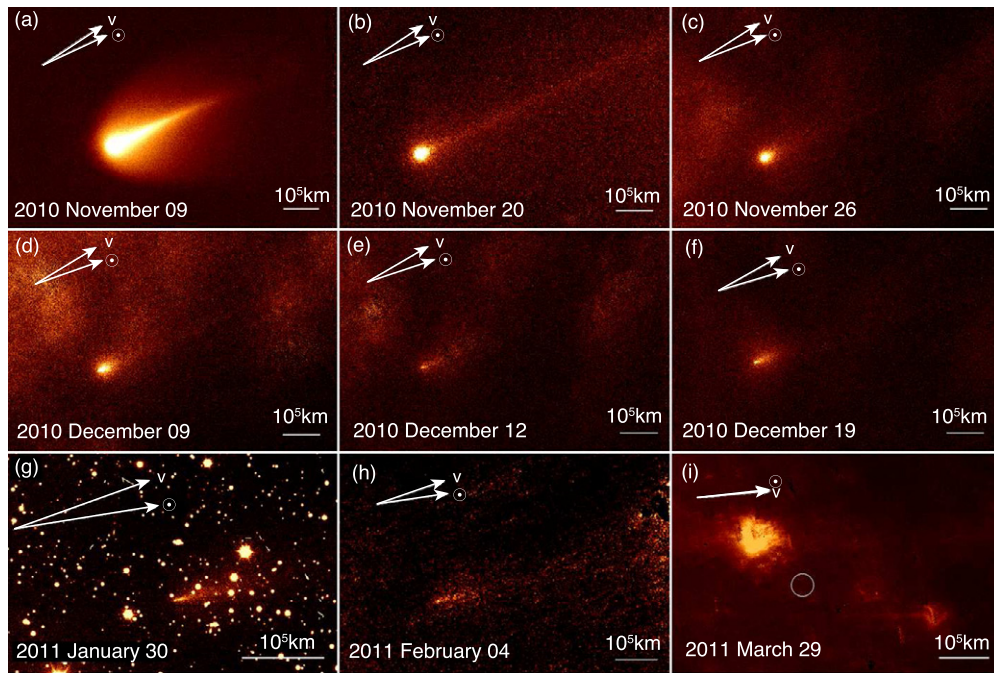
Figure 4. Time-series R_C-band images of V1 on (a) UT 2010 November 9, (b) November 20, (c) November 26, (d) December 9, (e) December 12, (f) December 19, (g) 2011 January 30, (h) February 04, and (i) March 29 in arbitrary brightness scale. These images have the standard orientation in the sky, that is, north is up and east is to the left. The field of view of the image is $9' \times 6'$ for panels (a)–(f) and panels (h)–(i) and $4.'5 \times 3'$ for panel (g). The cardinal directions are marked, as are the projected anti-solar direction ($\odot$) and the projected negative heliocentric velocity vector (V). The predicted position of the comet in panel (i) was illustrated by a circle whose radius corresponds to root-sum-of-squares of the three-standard deviation plane-of-sky error ellipse based on NASA/JPL ephemeris generator. There was no detectable object brighter than 20.0 mag in the predicted position. Note that the background of skies in panels (c)–(e) were largely contaminated by off-axis scattered light from Venus (smudge-like features in upper left of the images) while patchy features in panel (i) are remnants of bright stars and diffuse galaxies.
(A color version of this figure is available in the online journal.)

hardly visible in the second image (Figure 4(b)), and undetectable after the third day of our observation. On the other hand, the near-nucleus coma and the tail persisted until UT 2011 February 4 (Figures 4(a)–(h)). Finally, nothing was detected on UT 2011 March 29 (Figure 4(i)). We show the predicted position of the comet in Figure 4(i) using NASA/JPL's Horizons ephemeris generator.[12] No object brighter than 20.0 mag was detected. Assuming the geometric albedo of 0.04 (typical of comets), we determined an upper limit of the nuclear radius at ≈1850 m.

In Figure 4, we see that the orientation of the tail changed with time. To measure the position angles of the tail, we first applied the Larson–Sekanina filter (Sekanina & Larson 1984) in order to enhance fine-scale structures. We obtained profiles perpendicular to the projected orbit by averaging over 15–100 pixels parallel and 1–3 pixels perpendicular to the orbit. To each profile we fitted a Gaussian function. We then fitted a linear function to the peak of the Gaussian versus the distance from the nucleus. The slope and root-mean-square of the slope give us the position angle of the tail and the corresponding error bars (Jewitt et al. 2010). We plot the position angles as a function of the observed time (Figure 5). We initially compared these position angles with that of the anti-Sun vector (the extended Sun to comet radius vector as seen in the plane-of-sky), but found that the observed position angles significantly deviated from the anti-Sun vector. In addition, we compared them with synchrones, that is, the loci of dust particles emitted at specific dates with zero ejection velocity. In Figure 5, it is clear that synchrones reproduce the position angles over the

full range of dates observed, consistent with impulsive, rather than continuous, emission of dust. Specifically, we found best-fitting synchrone dates in the range from UT 2010 October 31 to November 3. These dates are consistent with a reported non-detection by Mr. Ikeya on November 1.8, one day before discovery of the comet on November 2.8 (Nakano & Ikeya 2010b). We conclude that an outburst occurred on V1 between UT 2010 October 31 and November 2.8, and most likely between November 1.8 and 2.8. In the remainder of this paper, we adopt UT 2010 November 2 as the time of outburst, after confirming that uncertainties in this date by up to two days do not materially change the interpretation below.

3.3. Photometry of the Near-nucleus Coma

The near-nucleus coma was visible as an approximately circular dust cloud. We obtained aperture photometry to study the material close to the nucleus with the aim of monitoring the comet's continued activity after its explosion. The photometry was performed using the *APPHOT* package in IRAF, which provides the magnitude within synthetic circular apertures projected onto the sky. We used apertures of fixed physical radius at the comet. A circular aperture of projected radius 15,000 km was used, corresponding to angular radii $8.''9$–$12.''3$. The apertures were large enough to be unaffected by seeing variations from night to night. Table 2 lists the measured R_C-band magnitudes, m_R.

We represent the absolute magnitude (i.e., the magnitude at a hypothetical point at unit heliocentric distance and observer's distance and at zero solar phase angle), by

$$m_R(1, 1, 0) = m_R - 5\log(r_h\Delta) - \beta\alpha, \qquad (1)$$
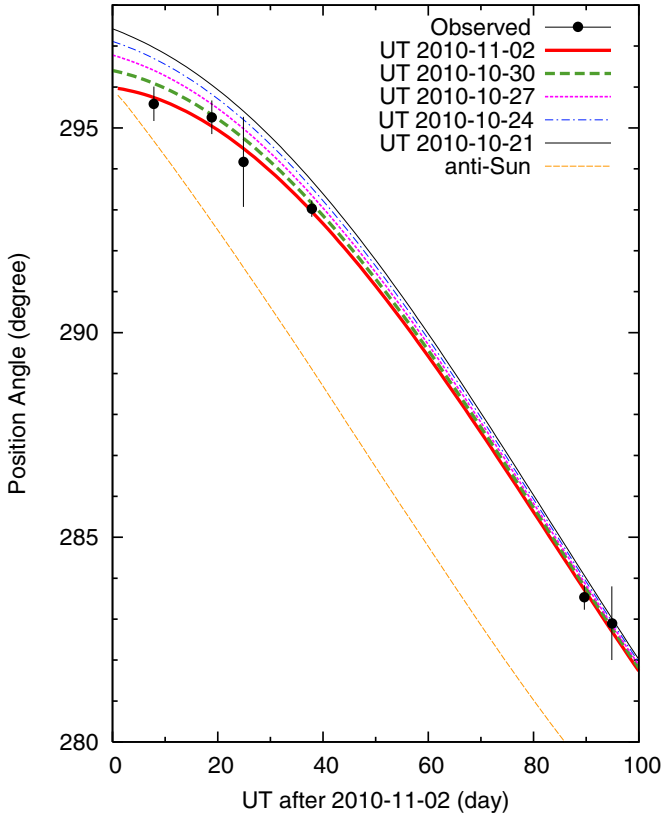
Figure 5. Position angles of the dust tail as a function of time showing changes caused by the viewing geometry. The measured position angles of the tail are indicated by filled circles with error bars denoting one standard deviation. Calculate position angles of different synchrones are also shown, labeled by the ejection time.

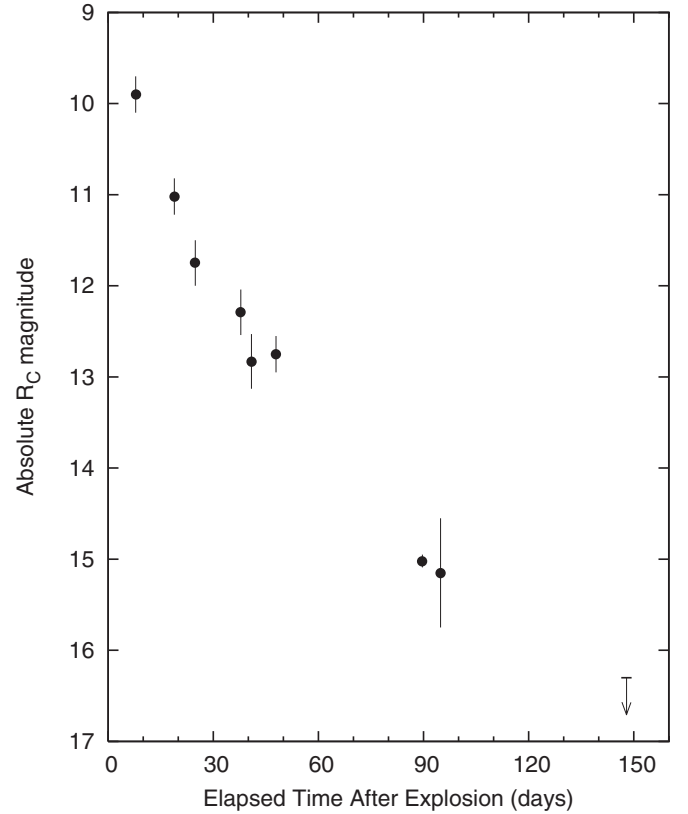(A color version of this figure is available in the online journal.)

Figure 6. R_C-band photometric evolution of V1's inner coma during UT 2010 November 9 and 2011 March 29 with a 15,000 km radius aperture. The horizontal axis is the elapsed time in day since the potential outburst date (UT 2010 November 2). The magnitude decreased by 0.06 a day over the period. Because no significant signal was detected on 2011 March 29, we show the upper limit of the magnitude.

Table 2
R_C-band Photometric Results

Median Time (UT)	m_R [error[a]]	$m_R(1, 1, 0)$
2010-11-09.87	13.45 [0.20]	9.90
2010-11-20.87	14.62 [0.20]	11.02
2010-11-26.87	15.38 [0.25]	11.75
2010-12-09.87	16.00 [0.25]	12.29
2010-12-12.87	16.56 [0.30]	12.83
2010-12-19.88	16.50 [0.20]	12.75
2011-01-30.66	18.93 [0.07]	15.02
2011-02-04.86	19.07 [0.60]	15.15
2011-03-29.94	>20.00	>16.27

Note. [a] Magnitude error 1σ.

where Δ and r_h are the observer's distance and the heliocentric distance in AU, β is the phase coefficient and α is the solar phase angle in degree. We used $\beta = 0.035$ mag deg^{-1} as determined from measurements of other comets (Lamy et al. 2004).

Figure 6 shows the absolute R_C-band magnitude of the dust coma as a function of time after UT 2010 November 2 (i.e., the day of the explosion). We show an upper limit from the last data taken with HCT. In the figure, we did not subtract the contribution to the flux from the nucleus. This contribution is unknown but probably negligible compared with dust cloud. We see that the coma magnitude decreased by ~5 magnitude (a factor of ~100) over ~80 days. The fading rate

of V1 (~0.06 mag day^{-1}) is slightly slower but approximately consistent with that of 17P/Holmes (0.08 mag day^{-1} when measured through a small photometry aperture, 2500 km: Stevenson & Jewitt 2012).

To understand the magnitude profile in Figure 6, we contrived a simple free expansion model in which dust particles expanded at a constant speed without any acceleration. In the model, we assumed that dust particles reached the projected aperture radius of our photometry (i.e., 15,000 km) throughout our observation. To validate the assumption, dust particles should have the initial speed >25 m s^{-1} to reach the projected radius on UT 2010 November 9 (we justify the assumption of the ejection speed in the following section). The number density of the cloud within the 15,000 km sphere decreases inversely with the cube of elapsed time. On the other hand, the length along the line-of-sight increases in direct proportion to elapsed time. As the result, the total number of particles within the 15,000 km sphere decreases as the inverse square of elapsed time. It suggests that the magnitude of the dust coma within the fixed physical radius can be described as $m_R(1, 1, 0) = 5\log(\Delta t) + m_0$, where Δt denotes the elapsed time and m_0 is a constant. We draw the line of $m_R(1, 1, 0) = 5\log(\Delta t) + m_0$ in Figure 7 adjusting m_0.

For comparison, we plot photometric results for 17P/Holmes also obtained with a circular aperture of projected radius 15,000 km (Table 3). The 17P/Holmes data were acquired at Kiso Observatory with the 2KCCD camera attached to the 1.05 m Schmidt telescope, and obtained from the public data archive, SMOKA. Although it is a crude model to describe the
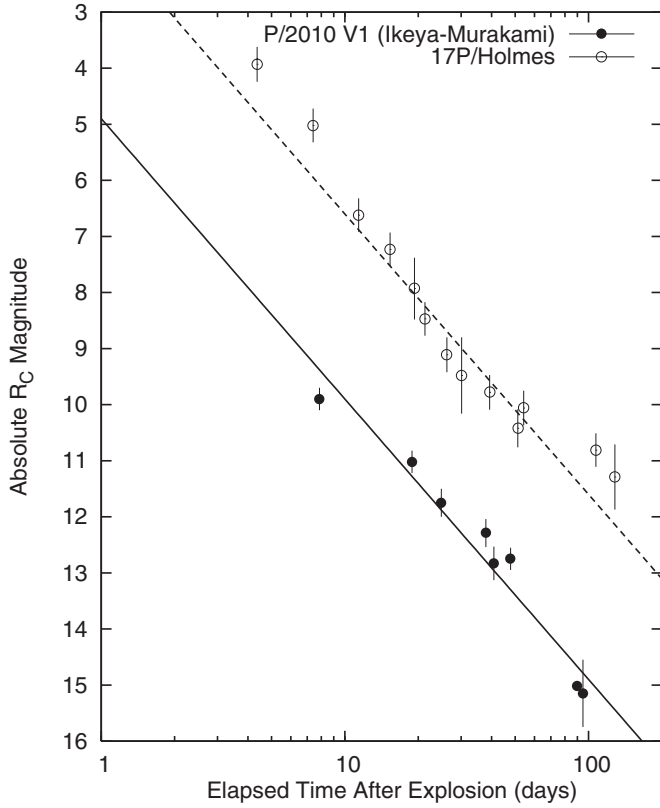
Figure 7. Comparison between R_C-band magnitude of the V1's inner coma and a free expansion model (lines) in logarithm scale. For comparison, we show R_C-band magnitude of 17P/Holmes with the same physical radius, where we assumed the onset time of the outburst on 2007 October 23.3 (Hsieh et al. 2010).

free expansion and there could be complicating factors such as dust disaggregation (Li et al. 2011; Sekanina 1982) and sublimation of icy grains (Stevenson & Jewitt 2012; Yang et al. 2009) as well as acceleration by solar radiation pressure, the fading trend is well matched by the free expansion model. We conclude that the bulk of the dust in V1 was ejected impulsively.

4. DISCUSSION

4.1. Dust Dynamical Model

For a better understanding of the unique morphology on UT 2010 November 9, we created model images of V1 based on a dynamical theory of dust grains. The dynamics of dust grains are determined both by the ejection speed (V_{ej}) and by the ratio of radiation pressure acceleration to solar gravity (β_{rp}). For spherical particles, β_{rp} is given by

$$\beta_{rp} = \frac{K Q_{pr}}{\rho_d a_d}, \quad (2)$$

where a_d and ρ_d are the particle radius and the mass density in the *MKS* system, and $K = 5.7 \times 10^{-4}$ kg m^{-2} is a constant. Q_{pr} is a radiation pressure coefficient the value of which depends on grain size, shape, structure and the optical constants of the grain material (Burns et al. 1979).

We applied a three-dimensional analysis to match the observed images, following the model in Ishiguro et al. (2007), Hanayama et al. (2012), and Ishiguro et al. (2013). We adopted a power-law function for the terminal speed of ejected dust

Table 3
Observational Circumstance and R_C-band Photometric Results of 17P/Holmes

Median Time	r_h	Δ	α	m_R [error[a]]	$m_R(1, 1, 0)$
2007-10-27.66	2.45	1.63	16.10	7.50 [0.31]	3.93
2007-10-30.71	2.46	1.62	15.30	8.56 [0.31]	5.02
2007-11-03.69	2.48	1.62	14.40	10.14 [0.31]	6.62
2007-11-07.63	2.49	1.62	13.50	10.73 [0.31]	7.23
2007-11-11.61	2.51	1.62	12.60	11.42 [0.55]	7.93
2007-11-13.62	2.52	1.63	12.30	11.97 [0.31]	8.47
2007-11-18.53	2.54	1.64	11.60	12.62 [0.32]	9.11
2007-11-22.43	2.55	1.65	11.30	13.00 [0.68]	9.48
2007-12-01.55	2.59	1.69	11.40	13.39 [0.31]	9.78
2007-12-13.58	2.64	1.78	12.90	14.24 [0.34]	10.42
2007-12-16.51	2.65	1.81	13.40	13.93 [0.31]	10.06
2008-02-07.57	2.88	2.54	19.70	15.82 [0.32]	10.81
2008-02-28.52	2.97	2.90	19.40	16.64 [0.58]	11.29

Note. [a] Magnitude error 1σ.

particles:

$$V_{ej} = V_0 \left(\frac{\beta_{rp}}{\beta_{rp,0}} \right)^{u_1} v, \quad (3)$$

where V_0 is the reference ejection speed of particles having $\beta_{rp,0} = 1$ and u_1 is the power index of the ejection speed. In a real comet the ejection speed will depend not only on β_{rp} but also on the location of the dust source on the nucleus, on the shape and porosity of the dust particles and perhaps on the ejection time within the outburst. The random variable v in Equation (3) reflects these uncertain factors. It follows the Gaussian probability density function, $P(v)$,

$$P(v) = \frac{1}{\sqrt{2\pi}\sigma_v} \exp\left[-\frac{(v-1)^2}{2\sigma_v^2} \right], \quad (4)$$

where σ_v is the standard deviation of v. In our computations, we limited the range $v - 1 < 2\sigma_v$ in order to avoid very fast particles. In addition, we set the minimum ejection speed to zero.

The number of dust particles at a given size is written:

$$N(a_d; t)\, da_d = N_0 \left(\frac{a_d}{a_0} \right)^{-q} da_d, \quad (5)$$

in the size range of $a_{min} \leqslant a_d \leqslant a_{max}$, where a_{min} and a_{max} are minimum and maximum particle size given by $a_{min} = 0.57/\rho_d \beta_{max}$ and $a_{max} = 0.57/\rho_d \beta_{min}$, respectively, and q is the power-index of the differential size distribution.

We imposed several constraints on the model. First, we considered that all dust particles were released impulsively on UT 2010 November 2, neglecting the possibility of weaker dust ejection before and after this date. This assumption is supported by our synchrone analysis and by the coma photometry as described above. Secondly, we supposed that ejected dust particles are compact in shape and can be represented by $Q_{pr} = 1$. This is a reasonable approximation for optically large ($2\pi a_d/\lambda \gtrsim 1$, where $\lambda \sim 0.64\,\mu$m is the wavelength) particles but is not strictly valid for optically small particles ($a_d \lesssim 0.2$–$0.3\,\mu$m) (see, e.g., Ishiguro et al. 2007). The dust mass density was assumed to be $\rho_d = 1000$ kg m^{-3}. We also assumed that the dust particles were ejected symmetrically with respect to the Sun–comet axis in a cone-shaped jet with a half-opening angle w, implying that the explosion occurred around the subsolar point of the nucleus.

Table 4
Dust Model Parameters

| Parameter	Input values	Best-fit (Envelope)	Best-fit (Tail+Coma)	Unit
u_1	0.1–0.9 with 0.1 interval	0.3 (fixed)	0.55 ± 0.1	$\cdots$
q	3.0–4.5 with 0.1 interval	4.0 ± 0.5	3.8 ± 0.1	$\cdots$
β_{max}	1.2, 1.5, 1.8	1.8	1.5	$\cdots$
β_{min}	$0.5, 1 \times 10^{-1}, 1 \times 10^{-2}, 1 \times 10^{-3}$	0.5	1×10^{-3} (fixed)	$\cdots$
V_0	150–600 with 30 interval	420 ± 30	315 ± 15	m s^{-1}
σ_v	0–0.5 with 0.1 interval	0.1 ± 0.05	0.5 ± 0.1	$\cdots$
ω	5–60 with 5 interval	30 ± 5	35 ± 10	deg

Finally, we assumed that, for particles of all sizes, the geometric albedo is 0.04 and the phase coefficient is $\beta = 0.035$ mag deg^{-1}.

We examined several key properties with which to constraint our dust model from the observed images. We noticed that the envelope has a more open shape in the anti-solar direction meaning that the width of the envelope was enlarged by increasing ejection speeds even as the envelope was stretched by the solar radiation pressure. Because smaller particles are more susceptible to radiation pressure, the envelope morphology suggests that small particles were ejected with higher speeds (see Figures 3 and 4(a)). From Equation (3), we can derive the power index of the ejection speed for the particles in the envelope, $u_1 = \log(w_1/w_2)/\log(\beta_1/\beta_2)$, where w_1 and w_2 are the apparent width of the envelope (proportional to the ejection speed projected on the celestial plane). We examined the width and the corresponding β_{rp} values from the image taken on 2010 November 9, finding that $u_1 = 0.30 \pm 0.05$ best fits the observed broadening of the envelope.

Separately, we found that the envelope did not extend more than ~4′.5 in our data. Particles with $\beta_{rp} > 2.5$ should have spread to the edge of the field of view in the time since ejection, while particles with $\beta_{rp} < 1$ would not match the observed extent. Through a test simulation for hemispherical ejection model (e.g., Reach et al. 2010, Section 6.1), we obtained $\beta_{rp} \sim$ 1.5. In the image on February, there is no obvious gap between the dust tail and the inner coma. From the evidence, we put the upper limits of $\beta_{min} \sim 1 \times 10^{-3}$.

Model images were produced in a Monte Carlo simulation by solving Kepler's equation including solar gravity and radiation pressure. We derived the above parameters to fit the surface brightness of the dust cloud on UT 2010 November 9, where prominent features (the envelope, tail, and coma) were detected. We created a number of simulation images using a wide range of parameters as listed in Table 4, and fitted the image from the outer parts to the inner parts. A two-component (i.e., envelope and tail+coma) model worked well for the fitting. We selected 20 sampling points in the envelope and found the optimum parameter sets first (envelope model). Then we subtracted the best-fit envelope model from the observed intensity, and selected 25 sampling points in the residual image, and derived the best-fit parameters to fit the tail and coma surface brightness (tail+coma model). The best-fit parameters are shown in Table 4. We tolerate intensity differences between the model and observation of up to 10%, and derived the errors in the table. Figure 8 shows the comparison between the observation and model. We produced the model contour through further tuning of the best-fit parameters within the error range. The distinctive morphology of the dust cloud is successfully reproduced by this two-component model.

The best-fit parameters suggest that the envelope consists of small particles ($\beta_{rp} = 0.5$–1.8 or $a_d = 0.3$–1 μm) with ejection

2 arcmin.
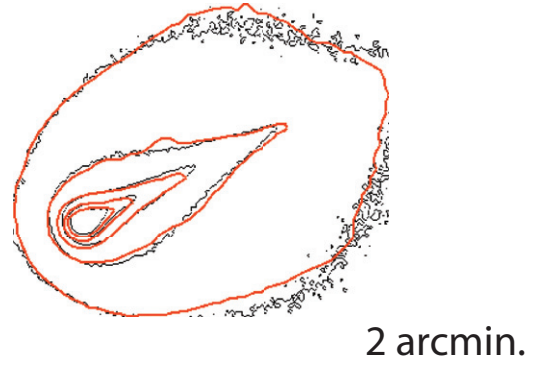
Figure 8. Comparison between the observed R_C-band image (thin lines) and one of our best-fit models (thick lines) on UT 2010 November 9. In this model, we used $u_1 = 0.3$, $q = 4.0$, $\beta_{min} = 0.5$, $\beta_{max} = 1.8$, $V_0 = 420$ m s^{-1}, $\sigma_v = 0.05$ and $w = 30°$ for the envelope, $u_1 = 0.52$, $q = 3.8$, $\beta_{min} = 1 \times 10^{-3}$, $\beta_{max} = 1.5$, $V_0 = 320$ m s^{-1}, $\sigma_v = 0.60$ and $w = 35°$ for the tail and coma. The contour levels are chosen arbitrary but the intervals are constant in linear scale. The field of view of these images is $9' \times 6'$.

(A color version of this figure is available in the online journal.)

speeds higher than in the coma and tail. The reference speed of particles in the envelope was $V_0 = 420 \pm 30$ m s^{-1}. With the range of β_{pr}, the ejection speed of the envelope particles turned out to be 290–500 m s^{-1}, where we adopted $\sigma_v = 0$ to derive the typical speed. On the other hand, the tail and coma consisted of a wide range of dust particles from sub-micron to submillimeter ($\beta_{rp} = 1 \times 10^{-3}$–1.5 or $a_d = 0.4$–570 μm) in size. Their ejection speeds are estimated to vary from 7–390 m s^{-1}. The effective radius, a_e, of dust particles in the coma is given by $a_e \approx \sqrt{0.4 \times 570} = 15 \ \mu$m. The ejection speed of a 15 μm particle is 52 ± 3 m s^{-1} from Equation (3), which is fast enough to reach the projected radius of 15,000 km during the time of our observation. This explains why the free expansion model can characterize the observed magnitude profile (Section 3.3).

We obtained the power index of β_{rp}-dependence of the ejection speed, $u_1 = 0.30 \pm 0.05$ in the envelope and 0.55 ± 0.10 in the tail and coma. Given the uncertainties, it is not clear that the difference between these estimates is formally significant. We note that the value $u_1 \sim 0.5$ is expected of dust particles accelerated by gas drag forces (Whipple 1951). The moderate slope for the envelope particles may suggest that small particles may be largely accelerated to reach the gas velocity.

We deduced the total mass of dust and the total kinetic energy by integrating with respect to particle size, as summarized in Table 5. The total dust mass is $M_d = 5.1 \times 10^8$ kg. With uncertainties in dust size (a_{min} and a_{max}) and its power index (q) as well as the photometric error (m_R), the derived mass is good to within a factor of four. The dust mass corresponds to a body 62 m in radius assuming mass density of $\rho_n = 500$ kg m^{-3}.

Table 5
Derived Physical Characteristics

Quantity	Envelope	Tail+Coma	Total	Unit
Speed[a]	420 ± 30	315 ± 15	$\cdots$	m s^{-1}
Particle radius	0.3–1	0.4–570	$\cdots$	10^{-6} m
Cross section	3.2 ± 0.3	7.2 ± 0.7	10.4 ± 1.0	10^{10} m^2
Mass	0.24	4.84	5.1	10^8 kg
Kinetic energy	2.2	2.8	5.0	10^{12} J

Note. [a] The speed of grains having $\beta = 1$ (radius 0.57 μm for density $\rho = 1000$ kg m^{-3}).

Table 6
Orbital Elements (Epoch 2455518.5, UT 2010-Nov-18.0)

Element	Value	Uncertainty (1σ)	Unit
Eccentricity, e	0.48803	0.00022	
Semi-major axis, a	3.0832	0.0016	AU
Perihelion distance, q_p	1.57854	0.00013	AU
Inclination, i	9.37832	0.00018	deg
Longitude of the ascending node, Ω	3.8155	0.0013	deg
Argument of perihelion, ω	152.396	0.014	deg
Time of perihelion passage, T_p	2455482.783	0.022	JED

This is $>0.004\%$ of the mass of a $r_n < 1850$ m spherical body (the upper limit of the nuclear radius). The total kinetic energy is $E_k = 5.0 \times 10^{12}$ J, or 1.2 kiloton of TNT, with the bulk of the energy carried by the tail and coma particles. Presumably, a comparable or larger energy was carried by gas in the initial explosion. The energy per unit mass is $E_k/M_d \sim 1 \times 10^4$ J kg^{-1}. The value is similar to that of 17P/Holmes (Li et al. 2011; Reach et al. 2010) and is about 10% of the energy released by the crystallization of amorphous water ice (9×10^4 J kg^{-1}).

The ejected mass could be contained in a surface layer on the nucleus having thickness (see, e.g., Li et al. 2011)

$$l = \frac{M_d}{4\pi r_n^2 f \rho_n}, \qquad (6)$$

where f is the fraction of the surface area of the nucleus that is ejected. We obtained $w = 30$–$35°$ to an accuracy of $\sim 10°$ from our model simulations, which suggests that the active area exists within $w \lesssim 30°$ from the sub-solar point. The area of the inferred active region is 2.9×10^6 m^2, corresponding to $f = 0.07$. Substituting these values gives $l > 0.35$ m. The ejected mass could be contained within a circular patch of the nucleus surface roughly 1 km in radius and 35 cm thick.

4.2. Dynamical Evolution of the Nucleus

Here we examine the orbital evolution of V1 to attempt to understand its recent history. Dynamical chaos imposes a fundamental limit to our ability to backward-integrate the motion of any comet; a small error in the initial conditions will grow exponentially on the Lyapunov time. There is additional uncertainty from the (generally poorly known) non-gravitational acceleration, which is induced in comets by recoil forces from the sublimation of ice. The non-gravitational parameters of V1 are not known. In the case of V1, there is in addition a relatively large uncertainty in the orbital elements because these were necessarily determined from observations taken over a short interval (only 80 days).

To investigate the past orbit, we consider many "clones," whose initial orbits follow a Gaussian distribution with the average values and the standard deviations provided by the NASA/JPL HORIZONS site (Table 6). Then the clone orbits are calculated and examined statistically. We generated 1,000 clones of V1 using the N-body integration package, Mercury (Chambers 1999), and calculated the orbital evolution over the past 10,000 yr. We set the non-gravitational force equal to zero.

Figure 9 shows the orbital evolution of five sample clones. They follow almost identical orbits for about 100 yr before present epoch, with perihelion fixed near 1.6 AU. Their Tisserand parameters drop below 3 and become Jupiter-family comets within 100–200 yr. Thus, V1 is likely to be a Jupiter-family comet which originated in the Kuiper-belt region. Comets

generally become active within ≈ 2.5 AU owing to sublimation. We examined the fraction of V1 clones which existed within 2.5 AU as visible comets. We found that all the V1 clones had perihelion <2.5 AU over the last 100 yr, dropping to 74% over 1000 yr and 19% in 10,000 yr. On this basis, it is clear that V1 is unlikely to be a new comet making its first appearance at small heliocentric distances. Therefore, the non-detection of V1 before 2010 is either a result of sky-survey incompleteness (unlikely, given the brightness of the comet) or a reflection of much reduced activity in previous orbits. We conjecture that, until the outburst on 2010 November 2, activity on the nucleus was largely stifled by a dust mantle, leading to low brightness and the non-detection of V1.

4.3. Comparison with Other Comets

Like V1, 17P/Holmes was discovered (in 1892) because of a dramatic outburst. Another outburst, in 2007, was well observed, revealing a spherical envelope, a detached blob, and a central coma (see, e.g., Watanabe et al. 2009; Reach et al. 2010). Total ejecta mass was estimated to be $(1 \sim 610) \times 10^{10}$ kg (Altenhoff et al. 2009; Reach et al. 2010; Ishiguro et al. 2010; Li et al. 2011; Boissier et al. 2012; Ishiguro et al. 2013). The expansion speed on the plane of the sky of the dust envelope particles was 554 ± 5 m s^{-1} (Lin et al. 2009; Montalto et al. 2008). Several other comets are known to have undergone huge photometric outbursts accompanied by circular envelopes. For example, 41P/Tuttle–Giacobini–Kresak experienced an outburst at 1.15 AU, and, before fading underwent second outburst at 1.25 AU from the Sun. It possessed an envelope (probably consisting of dust and gas; Sekanina 2008a) expanding at 300–700 m s^{-1} (Kresak 1974). 1P/Halley experienced a massive explosion in 1836 at 1.44 AU from the Sun. Similarly, 1P/Halley was enclosed by a circular envelope consisting of dust particles traveling at a speed of 575 ± 9 m s^{-1} (Sekanina 2008b). Only 17P/Holmes and V1 were observed with modern astronomical instruments (i.e., CCD) and the others were observed by photographic plates or naked eyes. We summarize the physical quantities of the outburst events at 17P/Holmes and V1 in Table 7. Although the magnitudes and heliocentric distances are different, the maximum speeds are similar to one another. Figure 10 shows the comparison between the 2010 V1 event (this work) and the 2007 17P/Holmes event (Reach et al. 2010; Lin et al. 2009). The dust size was not specified in Lin et al. (2009) and Montalto et al. (2008), but we regard it as sub-micron particles (i.e., $0.3^{+0.7}_{-0.2}$ μm) because only such small particles can be accelerated to the highest velocity and remain as sensitive scatterers in optical observations. Reach et al. (2010) provided the speeds for three different populations (core, blob and shell). Although the total dust mass and the kinetic energy
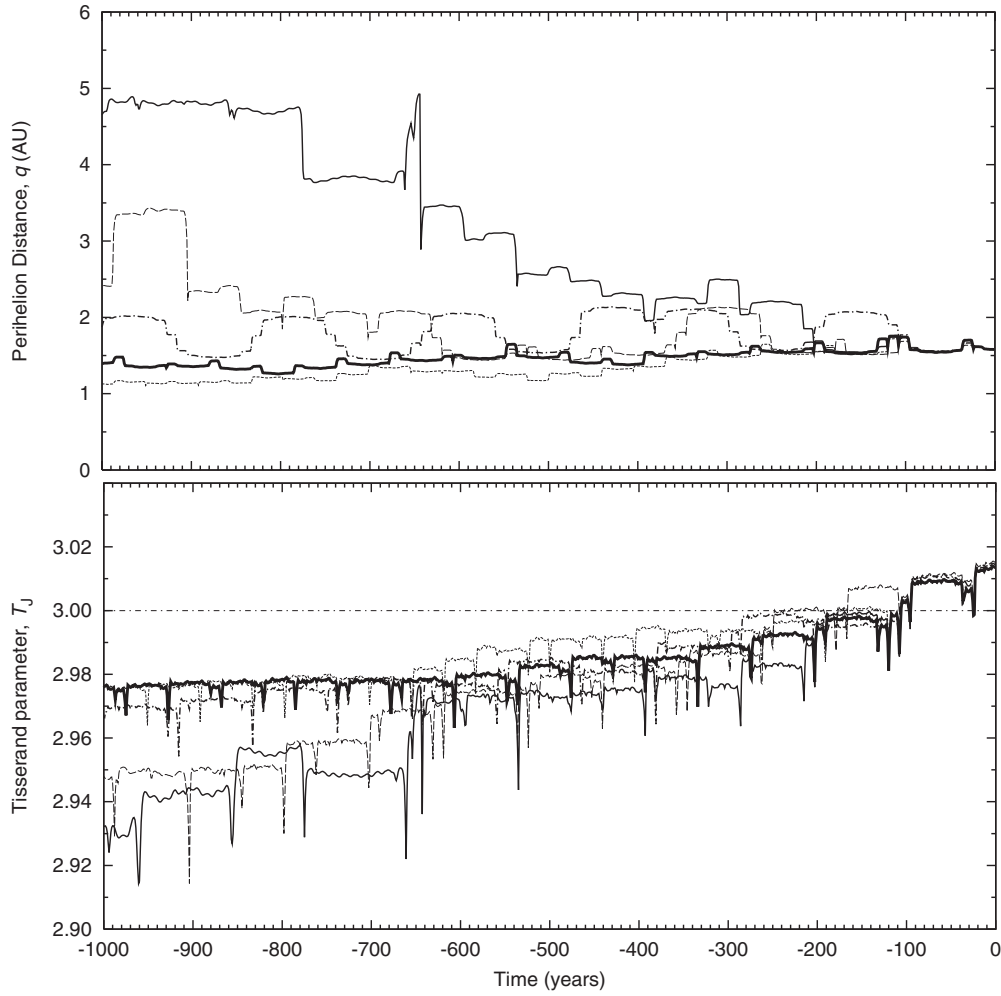
Figure 9. Examples of orbital evolution of V1 clone.
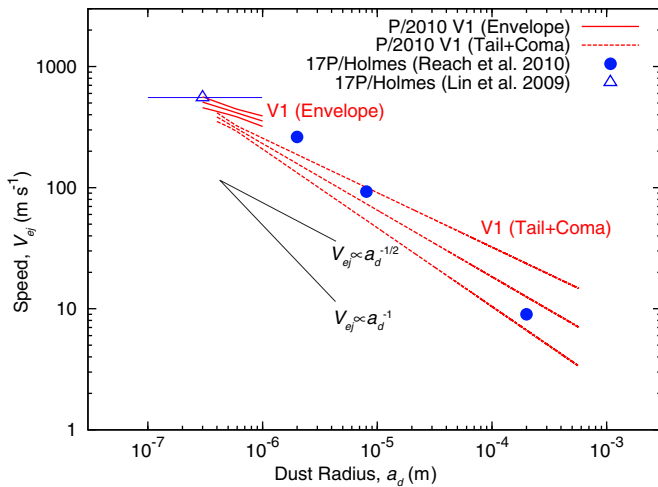
Figure 10. Comparison of speed between 17P/Holmes event in 2007 and V1 event in 2010. Three lines for V1 denote maximum, nominal, and minimum speed based on our model simulation (see V_0 and u_1 in Table 4. σ_v is not considered in this graph). Three filled circles are obtained from Reach et al. (2010). Open triangle is the projected speed of dust envelopes observed soon after the outburst (Montalto et al. 2008; Lin et al. 2009), where we assumed the particles size of sub-micron (i.e., 0.1–1 μm).

(A color version of this figure is available in the online journal.)

of these two events are different, the size–speed relationships are quite similar to one another.

Several possible mechanisms have been presented to explain the 17P/Holmes outburst; these include vaporization of pockets of more volatile ices such as CO_2 and CO (Schleicher 2009; Kossacki & Szutowicz 2011), the phase change of water from amorphous to crystalline ice (Sekanina 2009), thermal stress in the nucleus, or the polymerization of hydrogen cyanide (Gronkowski & Sacharczuk 2010). A plausible trigger is the crystallization of amorphous water ice (Prialnik et al. 2004). From Table 7, most of large-scale outbursts occurred after their perihelion passages, suggesting that a time-lag from conducted heat might trigger these outbursts.

The heat diffusion equation can be solved to give the distance over which heat can be transported by conduction, $\delta r = (\kappa P/\pi)^{1/2}$, where κ is the thermal diffusivity of the surface materials and P is the period of time over which conduction acts (Li et al. 2011). The applicable thermal diffusivity in comets is uncertain, depending on the unknown porosity of the material. Insulating solids typically have $\kappa \sim 10^{-6}$ m² s⁻¹ while $\kappa = 10^{-7}$ to 10^{-8} m² s⁻¹ maybe more appropriate for comets in which porous structure reduces the contact area between grains (Prialnik et al. 2004). If, as seems likely from the clone experiments, V1 has spent $\gtrsim 100$ yr inside 2.5 AU, conducted heat would reach a depth $\delta r \gtrsim 3$ to 10 m beneath the initial surface. Since $\delta r \gtrsim l$ (Equation (6)), it is quite plausible,

9

Table 7
Comparison between P/2010 V1 and 17P/Holmes Outbursts

Quantity	P/2010 V1	17P/Holmes	References for 17P/Holmes
a[a]	3.083	3.621	
e[b]	0.488	0.432	
i[c]	9.378	19.090	
q_p[d]	1.579	2.057	
r_h[e]	1.59	2.44	
r_N[f]	<1.85	1.71	Lamy et al. (2004)
Δt_p[g]	+20	+172	Hsieh et al. (2010)
$m_R(1, 1, 0)$[h]	5.97 ± 0.14	-1.12 ± 0.30	This work[p]
A[i]	$(1.0 \pm 0.2) \times 10^{11}$	$(7.1 \pm 2.2) \times 10^{13}$	This work[p]
$t_{\rm rise}$[j]	≈ 1	1.2 ± 0.3	Li et al. (2011)
$t_{\rm fade}$[k]	70	50	Stevenson & Jewitt (2012)
M_d[l]	5.1×10^8	$(1 \sim 610) \times 10^{10}$	Li et al. (2011); Ishiguro et al. (2013)
$V_{\rm max}$[m]	500 ± 40	554 ± 5	Lin et al. (2009)
E_k[n]	5.0×10^{12}	$(1.2 \sim 1400) \times 10^{14}$	Li et al. (2011); Reach et al. (2010)
E_k/M_d[o]	1×10^4	1.2×10^4	Reach et al. (2010)

Notes.
[a] Semimajor axis in AU.
[b] Eccentricity.
[c] Inclination in degree.
[d] Perihelion distance in AU.
[e] Heliocentric distance at the time of outburst in AU.
[f] Radius of nucleus in km.
[g] Onset time after perihelion passage in days.
[h] Absolute R_C-band magnitude.
[i] Total cross section of dust cloud in m^2.
[j] Rise time in days.
[k] Fade time when the magnitude decreased by 4 mag in days.
[l] Ejecta mass in kg.
[m] Maximum speed of ejecta in m s^{-1}.
[n] Kinetic energy in J.
[o] Kinetic energy per unit mass in J kg^{-1}.
[p] These were obtained by ourselves using images taken at Kiso observatory.

although far from proved, that the outburst was triggered by the action of conducted heat through the crystallization of buried amorphous ice.

5. SUMMARY

From our research on V1, we find the following.

1. Several observations show that V1 underwent an explosive ejection in late 2010. The changing position angle of the dust tail is closely matched by synchrone trajectories for ejection dates between UT 2010 October 31 and November 3. The near-nucleus coma faded steadily at ~ 0.06 mag day^{-1}, distinct from any steady-state behavior. The non-discovery of this nearby, bright comet before 2010 is naturally explained by the outburst interpretation.

2. The V1 dust cloud had two distinct components. The envelope consisted of small grains (radii 0.3–1 μm) expanding at a maximum speed of 500 ± 40 m s^{-1}. The tail and coma were composed of a wider range of dust particles (radii 0.4–570 μm) and expansion speeds of 7–390 m s^{-1}.

3. The ejecta mass in solids is 5.1×10^8 kg and the kinetic energy is 5.0×10^{12} J. Although the mass and energy are orders of magnitude smaller than in 17P/Holmes, the energy per unit mass ($\sim 1 \times 10^4$ J kg^{-1}) is similar.

4. The sudden ejection and the derived energy per unit mass of the ejecta are consistent with runaway crystallization of buried amorphous ice as the source of energy to drive the outburst.

REFERENCES

Altenhoff, W. J., Kreysa, E., Menten, K. M., et al. 2009, A&A, 495, 975
Boissier, J., Bockelée-Morvan, D., Biver, N., et al. 2012, A&A, 542, A73
Brown, M. E., Bouchez, A. H., Spinrad, A. H., & Johns-Krull, C. M. 1996, AJ, 112, 1197
Burns, J. A., Lamy, P. L., & Soter, S. 1979, Icar, 40, 1
Capria, M. T., Cremonese, G., & de Sanctis, M. C. 2010, A&A, 522, A82
Chambers, J. E. 1999, MNRAS, 304, 793
Combi, M. R., & Delsemme, A. H. 1980, ApJ, 237, 633
Gronkowski, P., & Sacharczuk, Z. 2010, MNRAS, 408, 1207
Hanayama, H., Ishiguro, M., Watanabe, J.-I., et al. 2012, PASJ, 64, 134
Holmberg, J., Flynn, C., & Portinari, L. 2006, MNRAS, 367, 449
Hsieh, H. H., Fitzsimmons, A., Joshi, Y., Christian, D., & Pollacco, D. L. 2010, MNRAS, 407, 1784
Ishiguro, M. 2008, Icar, 193, 96
Ishiguro, M., Kim, Y., Kim, J., et al. 2013, ApJ, 778, 19
Ishiguro, M., Sarugaku, Y., Ueno, M., et al. 2007, Icar, 189, 169
Ishiguro, M., Watanabe, J.-I., Sarugaku, Y., et al. 2010, ApJ, 714, 1324
Jewitt, D., Weaver, H., Agarwal, J., Mutchler, M., & Drahus, M. 2010, Natur, 467, 817

Kim, J., Ishiguro, M., Hanayama, H., et al. 2012, ApJL, 746, L11
Kossacki, K. J., & Szutowicz, S. 2011, Icar, 212, 847
Kresak, L. 1974, BAICz, 25, 293
Lamy, P. L., Toth, I., Fernandez, Y. R., & Weaver, H. A. 2004, in Comets II, ed. M. C. Festou, H. U. Keller, & H. A. Weaver (Tucson, AZ: Univ. Arizona Press), 223
Landolt, A. U. 1992, AJ, 104, 1, 340
Landolt, A. U. 2009, AJ, 137, 4186
Levison, H. F., & Duncan, M. J. 1997, Icar, 127, 13
Li, J., Jewitt, D., Clover, J. M., & Jackson, B. V. 2011, ApJ, 728, 31
Lin, Z.-Y., Lin, C.-S., Ip, W.-H., & Lara, L. M. 2009, AJ, 138, 625
Mink, D. J. 1997, in ASP Conf. Ser. 125, Astronomical Data Analysis Software and Systems VI, ed. G. Hunt & H. E. Payne (San Francisco, CA: ASP), 249
Monet, D. G., Levine, S. E., Canzian, B., et al. 2003, AJ, 125, 984
Montalto, M., Riffeser, A., Hopp, U., Wilke, S., & Carraro, G. 2008, A&A, 479, L45
Nakano, S., & Ikeya, K. 2010a, IAUC, 9175, 1

Nakano, S., & Ikeya, K. 2010b, IAUC, 9183, 3
Oke, J. B., Cohen, J. G., Carr, M., et al. 1995, PASP, 107, 375
Prialnik, D., Benkhoff, J., & Podolak, M. 2004, in Comets II, ed. M. C. Festou, H. U. Keller, & H. A. Weaver (Tucson, AZ: Univ. Arizona Press), 359
Reach, W. T., Vaubaillon, J., Lisse, C. M., Holloway, M., & Rho, J. 2010, Icar, 208, 276
Schleicher, D. G. 2009, AJ, 138, 1062
Sekanina, Z. 1982, in Comets, ed. L. L. Wilkening (Tucson, AZ: Univ. Arizona Press), 251
Sekanina, Z. 2008a, ICQ, 30, 3
Sekanina, Z. 2008b, ICQ, 30, 63
Sekanina, Z. 2009, ICQ, 31, 5
Sekanina, Z., & Larson, S. M. 1984, AJ, 89, 1408
Stevenson, R., & Jewitt, D. 2012, AJ, 144, 138
Watanabe, J.-I., Honda, M., Ishiguro, M., et al. 2009, PASJ, 61, 679
Whipple, F. L. 1951, ApJ, 113, 464
Williams, G. V. 2010, IAUC, 9189, 2
Yang, B., Jewitt, D., & Bus, S. J. 2009, AJ, 137, 4538